

1 **Original Article**

2

3 **An EMG-driven biomechanical model of the canine cervical spine**

4 M. Alizadeh ^{a*}, G.G. Knapik ^a, J.S. Dufour^a, C. Zindl^b, M.J. Allen^{b,c}, J. Bertran^c, N. Fitzpatrick^d,
5 W.S. Marras^a

6

7 ^a *Spine Research Institute, The Ohio State University, 520 Baker Systems, 1971 Neil Avenue.,*
8 *Columbus OH 43210 USA*

9 ^b *Surgical Discovery Center, Department of Veterinary Medicine, University of Cambridge,*
10 *Madingley Road, Cambridge, CB3 0ES, UK*

11 ^c *Department of Veterinary Clinical Sciences, The Ohio State University, Columbus, Ohio 43210*
12 *USA*

13 ^d *Fitzpatrick Referrals, Eashing, Surrey GU7 2QQ, UK*

14

15 * Corresponding author.

16 *E-mail address: Alizadeh.3@osu.edu (Name: Mina Alizadeh).*

17 *Postal address: The Ohio State University, Spine Research Institute, 1971 Neil Avenue, Room*
18 *520, Columbus, OH 43210*

19

20

21

22

23 **Abstract**

24 *Background:* In spite of the frequency of cervical spine injuries in canines, a biomechanical
25 understanding that enables one to investigate the risk of neck disorders associated with physical
26 activities and external loads, and surgical procedures has not been developed. The purpose of
27 this effort was to develop an EMG-driven dynamic model of the canine cervical spine to assess
28 the load profile imposed upon the canine neck during physical exertions.

29 *Methods:* a canine subject was recruited in this investigation in order to collect subject specific
30 data. Reflective markers and motion capture system were used for kinematic measurement;
31 surface electrodes were used to record electromyography signals, and with the aid of force plate
32 kinetics were recorded. 3-D model of the canine subject were reconstructed from MRI dataset.
33 Muscles lines of action were defined through a new technique with the aid of 3D white light
34 scanner.

35 *Results:* The reliability of the model was investigated by comparing the resultant dynamic
36 measured external moment to the predicted internal moment in both the sagittal and axial planes
37 via correlation coefficient (R^2) and average absolute error (AAE). The model performed well
38 with a 0.73 weighted R^2 value in all three planes. The weighted average absolute error of the
39 predicted moment was less than 10% of the external moment.

40 *Interpretation:* The proposed model is a canine specific forward-dynamics model that precisely
41 tracks the canine subject head and neck motion, calculates the muscle force generated from the
42 twelve major moment producing muscles, and estimates resulting loads on specific spinal
43 tissues.

44 *Keywords:* dog; neck; electromyography, dynamic, kinematics.

45

46 **1. Introduction**

47 The canine's cervical spine is particularly susceptible to trauma because of the large
48 moment generated by the head relative to the base of the spine (Breit and Künzel, 2004; Crisco et
49 al., 1990; Jeffery et al., 2013). In order to develop a better understanding of preventive strategies
50 and effective therapeutic interventions, a more quantitative appreciation of canine cervical spine
51 biomechanics is desirable, since a detailed biomechanical knowledge of the frequent sites of
52 cervical spine injury is required. Biologically-assisted biomechanical models provide a viable
53 environment to understand spine tissue loading in vivo. Once developed, these models are
54 capable of helping to understand potential injury risk by accounting for how muscles are
55 dynamically recruited and how the patterns of muscles recruitments collectively impose forces
56 on tissues under various daily activities. It is believed this model will significantly help to
57 understand canine cervical spine kinematics which is still not well understood (Johnson et al.,
58 2011). In addition, such model can help us understand the implications of contemplated surgeries
59 on the biomechanical behavior of the spine. Beyond the application of canine cervical spine
60 biomechanical models in veterinary medicine, these models could be used further to better
61 understand complex biomechanical relationships and the knowledge gained can be translated and
62 applied to human spine models. In vivo studies on canines can be easily conducted and used to
63 validate overall subject-specific model outputs. Moreover, this model will provide a suitable
64 platform to explore the validity of canine cervical spine models that have been employed
65 extensively for investigating effects of spinal instruments developed for human spine (Autefage
66 et al., 2012; Lim et al., 1994; Sharir et al., 2006; Sheng et al., 2010). Several human cervical
67 spine models have been developed and validated to better understand the mechanical loads on
68 the human spine (Horst et al., 1997; Hyeonki Choi, 2010; Jager et al., 1996; Lopik and Acar,

69 2007; Snijders et al., 1991; Stemper et al., 2004; Vasavada et al., 1998). In spite of the high
70 frequency of spinal injuries observed in canines (Foss et al., 2013; Jeffery et al., 2013), attempts
71 to develop models for the canine cervical spine have been lacking, to our knowledge.

72 Since the muscles surrounding the spine are the major contributors to spine loading, a
73 critical component of a biomechanical model is the ability for the model to accurately estimate
74 muscle force. Since the cervical spine and its muscles are a statistically indeterminate system,
75 cervical spine biomechanical models utilize one of two approaches to compute muscle forces:
76 inverse dynamics or biologically-assisted (electromyography or EMG-driven) techniques, (Choi
77 and Vanderby Jr, 1999; Cholewicki and McGill, 1994). In spite of the popularity of inverse
78 dynamic driven models, they have fairly significant shortcomings. Inverse dynamics models are
79 appropriate in highly dynamic (impulse) loading situations such as whiplash, where muscles do
80 not have enough time to activate and alter tissue loading (Huber, 2013) and for static exertions.
81 However, during activities of daily living, which represent the vast majority of lifetime
82 exposures, inverse dynamics models cannot account for the complex co-contraction of antagonist
83 muscles surrounding the spine. Studies have shown that significant muscle coactivations occur in
84 the muscles surrounding the lumbar spine in humans and that accounting for these coactivities
85 profoundly increases spinal load predictions compared to inverse dynamic models that assume
86 no coactivity (Granata and Marras, 1995). It has been suggested that muscle forces, on average,
87 can be as high as 218% greater in lateral bending and 123% greater in flexion/extension in EMG-
88 driven models of the lumbar spine compared to inverse dynamic models (Cholewicki et al.,
89 1995). It is expected that these underestimations would be even greater in the cervical spine since
90 the relatively small mass of the head may require larger amounts of coactivity to protect it from
91 perturbations and keep it in a stable state. We expect that inverse dynamics models would

92 severely underestimate cervical spine tissue loading (Hyeonki Choi, 2010). Hence, the EMG-
93 driven biomechanical modeling approach would be expected to enable a much better estimation
94 of spinal loads since it accounts for realistic antagonist muscle cocontraction during dynamic
95 physical activities. In addition, EMG-driven models also account for the individual variability
96 across subjects and conditions in muscle recruitment.

97 Therefore, the objective of this study was to develop a canine specific EMG-driven
98 cervical spine model that would be sensitive to dynamic physical exertions of the cervical spine
99 and capable of accurately predicting internal moments and spinal tissue loading profiles.

100

101 **2. Methods**

102 2.1 Modeling approach

103 We applied well developed human spine modeling concepts to to the development of a
104 canine cervical spine biomechanical model (Marras and Granata, 1997; Theado et al., 2007). In
105 order to build the EMG-driven model, several experimentally measured parameters including
106 kinematic information, kinetic profiles, muscles of canine cervical spine structure, and EMG
107 signals were incorporated as model inputs to predict the resultant internal moments and spinal
108 loads as model outputs (Fig.1). The underlying logic of the model assumes that the key to precise
109 estimation of spinal loads is to understand how the internal tissues respond to physical exertions
110 and activities and estimate tissues force contributions to the system. Below we briefly describe
111 how the model inputs were acquired and implemented into the model.

112 2.1.1 Muscle modeling

113 Muscle function is represented as a three-dimensional vector function of force
114 magnitude and force direction via dynamic muscle lines of action. Dynamic tensile force of a
115 muscle (j) is estimated (eq.1) as the product of muscle gain ratio ($GainRatio_j$), EMG (EMG_j),
116 muscle cross-section area ($Area_j$), while taking into account the force-length ($f(L_j(t))$) and
117 force-velocity ($f(V_j(t))$) relationship of the muscles (Theado et al., 2007). Moment generated
118 by the muscles (M) were calculated via summation of vector products between muscle (j) tensile
119 force (F) and its moment arm (r) at every time point during the dynamic trial (eq.2) (Theado et
120 al., 2007).

121 Muscle moment arm is defined as the perpendicular distance of muscle line of action
122 from the joint axis of rotation (Vasavada et al., 1998). The model is operating such that the gain
123 ratio for each muscle was predicted within a calibration trial, in order to personalize muscle
124 forces for the canine subject similar to the technique that was developed by Dufour et al. (2013)
125 for human lumbar spine muscles. A simple flexion/extension trial was selected as a calibration
126 trial. Once these parameters for each muscle were specified, they were applied to analyze other
127 trials performed by the canine subject such as lateral bending and axial rotation tasks. In order to
128 accurately estimate muscle gain ratio, an optimization algorithm had been used to minimize error
129 between muscles' internal moments and external moments about cervical spine joints. Internal
130 moments included those generated by muscles and ligaments while external moments included
131 those imposed by external force measured from the force plate and the inertial contributions of
132 the head and vertebral bodies. Based on the anatomical properties of muscles in this model, the
133 objective function of calibration algorithm aimed to minimize moment prediction errors in two
134 joints, C1/C2 and C7/T1. The boundary conditions for the calibration procedure used here were
135 originally developed for the human lumbar spine. However, previous studies have shown

136 relatively similar muscle parameters between humans and canines (McCully and Faulkner,
137 1983). Therefore, these parameters should serve as a good starting point until boundaries for
138 normal canines can be developed.

$$F_j(t) = GainRatio_j \cdot Area_j \cdot EMG_j(t) \cdot f[L_j(t)] \cdot f[V_j(t)] \quad (1)$$

$$\vec{M} = \sum_{j=1}^{10} \vec{r}_j(t) \times \vec{F}_j(t) \quad (2)$$

139 Since there is currently a lack of comprehensive canine neck muscle properties to approximate
140 muscle lines of action and cross-sectional areas, the best technique for determining these
141 parameters for this model had to be determined. Medical imaging techniques and cadaveric
142 experiments are two of the most well established methods to measure muscle moment arms and
143 to define muscle line of action (Dumas et al., 1991; Macintosh and Bogduk, 1991; Németh and
144 Ohlsén, 1986). However there are many sources of inaccuracies associated with these
145 techniques. First, and the most probable shortcoming was that of the partial volume effect
146 phenomena, where a large bias can be introduced in measured parameters on medical images
147 (Soret et al., 2007). Second, scan planes are generally perpendicular to the scan table while the
148 direction of the muscles are most probably oblique to the scan plane, consequently CSA derived
149 from images are typically overestimated (Jorgensen et al., 2003). Adjusting the CSA for muscle
150 fiber angle can reduce this error, however, muscle fiber directions are often not detectable via
151 MRI. Considering individual variability across subjects, it is impossible to correct CSA for the
152 subject-specific models with medical images. Third, distinguishing muscles and separating them
153 from one another requires a thorough knowledge of cross-sectional anatomy as well as powerful
154 MRI imaging to be able to visually differentiate muscles. In order to reduce error introduced by

155 these limitations in the model, an alternative approach was investigated to determine muscle line
156 of action.

157 The application of a three-dimensional white light scanner (3DWLS) (Artec Eva, Artec,
158 Palo Alto, CA, USA) to determine muscle lines of action while minimizing medical imaging
159 shortcomings was investigated. The Artec Eva 3D scanner consists of a portable camera that
160 dynamically captures 3D geometry data and surface information at up to 15Hz. It is an ideal tool
161 for medical scanning purposes because: a) the 3D scanner is able to provide a 3D view of an
162 object to help identify cervical spine muscles in their complex geometrical arrangement; and, b)
163 the scanner is capable of providing high resolution images while capturing texture at high speed.
164 One advantage of this approach is that measurements such as fiber angles and muscle cross-
165 sections are taken directly from intact muscles without disturbing muscle attachments. Therefore,
166 more accurate measurements in comparison to previous direct dissection cadaveric studies would
167 be expected. A cadaver dog, euthanized for another research protocol unrelated to this study was
168 used to test the proposed technique for determining canine cervical muscle lines of action. The
169 cadaver dog was relatively similar to the canine subject we recruited for model development in
170 many aspects such as breed, weight and size.

171 The dog specimen dissection process started by removing the skin and underlying fatty
172 layers until most of the superficial muscle was exposed. Then, the 3D scanner was used to scan
173 the exposed muscle. Next, every single muscle in the neck region was removed carefully one at a
174 time, and the 3DWLS was used to capture the surface information of the next layer of exposed
175 intact muscle. The 3DWLS data was then post processed to evaluate the variability of the fiber
176 directions throughout the length of each muscle. Muscle volume was then defined as a volume
177 between two consecutive scans obtained in the order as described previously. Each muscle's line

178 of action was then approximated by the three dimensional centroid path of that muscle (Jaeger et
179 al., 2011). The muscle centroid line was achieved by connecting the central points of the muscle
180 cross-section in transverse planes. Those planes were defined as surfaces parallel to the vertebral
181 bodies' endplates with small distance as much as 5 mm from each in order to increase the
182 accuracy (Jaeger et al., 2011). Finally, to reduce modeling complexity for this first stage, a
183 straight line was fitted to the centroid path obtained by multiple planes and further used as the
184 straight muscle line of action.

185 Among the many muscles in the neck, six pairs representing the power producing
186 muscles were selected for modeling purposes. Muscles were chosen based on their moment arm
187 length, their cross-sectional area, and their accessibility via surface electromyography electrodes.
188 These twelve muscles (six muscle pairs), left/right sternomastoid, left/right obliquus capitis,
189 left/right splenius, left/right biventer, left/right complexus, and left/right longissimus lines of
190 action are shown in Figure 6. As mentioned earlier, we had recorded EMG signals for only four
191 pairs of muscles while there are six pairs of muscles in the model. Anatomically, splenius is
192 located dorsal to the biventer and complexus, with larger cross-sectional area and moment arm
193 compared to muscles underneath such as the biventer and complexus. This indicated that more
194 activation expected to be seen from splenius than biventer and complexus. Considering the
195 capability of surface electrodes on detecting different signals, it was not practical to locate
196 separate electrodes for splenius, biventer and complexus. Therefore, we recorded splenius
197 activity by EMG electrodes and we assumed the same recruitment pattern shape would apply to
198 biventer and complexus.

199 2.1.2 Geometry reconstruction

200 In order to generate the subject-specific anatomical model, the canine subject
201 underwent MRI imaging. A series of image processing operations were then performed on the
202 MRI images in order to obtain a detailed three-dimensional model of the canine cervical spine
203 (Skull - T1). The head and neck posture then were realigned to match the neutral standing
204 posture.

205

206 2.1.3 Ligaments and intervertebral disc modeling

207 Ligaments were modeled as passive force vectors located between two points
208 representing ligament attachment points. Ligament attachments in the model were adopted
209 based on anatomy literature (Kumar, 2012). The nuchal ligament, dorsal atlanto-occipital
210 membrane, lateral atlanto-occipital membrane, dorsal atlanto-axial ligament, ventral atlanto-axial
211 membrane, alar ligament, transverse atlantal ligament, apical ligament, alar ligament, apical
212 ligament, ventral longitudinal ligament, dorsal longitudinal ligament, yellow ligament,
213 interspinous ligament, and capsular ligament were all incorporated in the model. The width of
214 the ligament was represented using multi force vectors to ensure that the force could encompass
215 all the physiological width of the ligament. Due to the lack of canine ligament properties, human
216 cervical spine ligament properties were used in the model instead (Han et al., 2012).
217 Intervertebral disc geometry at each level was reconstructed from the MRI dataset and its
218 material properties obtained from the literature (Zimmerman et al., 1992). They were modeled as
219 three dimensional spring dampers located at the center of the disc space for each motion
220 segment. Therefore, at each spinal joint there is an intervertebral disc and anatomically match
221 ligaments in order to stabilize the joint. The atlanto-occipital and atlanto-axial are two complex
222 joint with a shared common joint capsule. Due to modeling limitations, assumptions were taken

223 to construct these joints. Cartilage at these joints was modeled as three dimensional spring
224 dampers with stiffness properties similar to cartilage stiffness (Jaumard et al., 2011). In addition,
225 with a defined contact forces at these joints the vertebral bodies distance were preserved without
226 increasing spinal load drastically. The final 3D dynamic model of canine cervical spine is shown
227 in Figure.2.

228

229 2.2 Modeling approach

230 2.2.1 Experimental tasks and training

231 A skeletally mature male hound (26.0 kg body weight) served as a subject in this
232 investigation. The dog was examined by a veterinarian and documented to be healthy, with no
233 evidence of joint or spinal disease. The dog was housed in a room with other dogs and was fed
234 a standard laboratory dog chow with water *ad libitum*. During the three weeks before the data
235 collection, the dog was trained using food treats to allow for passive manipulation of the head
236 and neck via a soft head collar (Gentle Leader, Suffolk, UK). Beginning from the neutral
237 position, the head and neck were slowly moved through a range of motion from full extension
238 (nose pointing up towards the ceiling) to full flexion (nose down towards the floor).
239 Movements were then repeated for side to side motions and for oblique motions. After going
240 through all motion sequences, a latex resistance band (TheraBand, Akron, OH, USA) was
241 attached to the head collar around the mandibular region and the end of the resistance band was
242 manually fixed on the floor, so that no traction was applied with the head in neutral position.
243 The sequence of passive head/neck movements was then repeated with the resistance band in
244 place. In order to slowly acclimate the dog to the resistance, training during the first week was

245 carried out with a band of medium resistance and during subsequent training sessions (week 2
246 and 3) and at the testing day with a band of significantly higher resistance.

247

248 2.2.2 Subject

249 One trained dog was enrolled in this experiment to perform several exertion trials in a room
250 equipped with a motion capture system and force plate. The experimental procedures for this
251 study were reviewed and approved by the local institutional animal care and use committee
252 (IACUC). The dog was acclimated to the experiment space 15-20 minutes before subject
253 preparation. In order to activate muscles, the dog was required to pull against a latex band
254 attached between its collar and the force plate during various exertion trials ranging from simple
255 flexion/extension to more complex exertions including axial rotation and lateral bending similar
256 to the training movements (Fig.3). During the experiment, the dog was encouraged to follow
257 food treats in the hand of the trainer to resemble the training procedure.

258

259 2.2.3 Data collection system (Apparatus)

260 Bipolar surface electrodes were placed over 8 neck muscles (four pairs of muscles). EMG data
261 was collected with a MA300-XVI Advanced Multi-channel EMG System (Motion Lab Systems
262 Incorporated, Baton Rouge, Louisiana, USA) at 1000 HZ collection frequency. The latex
263 resistance band force and moment were measured via a force plate (Bertec 4060A; Bertec,
264 Worthington, OH, USA). An OptiTrack optical motion capture system (NaturalPoint, Corvallis,
265 OR, USA) with 24 Flex 3 infrared cameras was used to capture optical marker locations during
266 the experiment via OptiTrack's Motive software. Custom software developed at the Ohio State
267 University Spine Research Institute was used to record analog signals through a NI USB-6225

268 Data Acquisition Device (National Instruments, Austin, TX, USA) and to control and sync
269 optical data collection.

270

271 2.2.4 Kinematic and kinetic data acquisition

272 Three reflective markers (optical) were attached to the bony landmarks of head: 1) left frontal
273 process, 2) right temporozygomatic bone, and 3) left nasal bone. Three more markers were
274 attached to a small solid panel made of plastic that was tightly secured to the back of the dog to
275 serve as a rigid body. Three more reflective markers were glued to the neck approximately on the
276 spinous process of C2, C5 and C7 and two more on the head of the scapula to represent shoulder
277 movement (Fig.4). The optical marker locations were recorded during each trial by the motion
278 capture system. Optical marker position data were then used to calculate the kinematics of the
279 head, neck and back referenced to the ground in a neutral posture which was recorded prior to
280 experimental tasks. Developing a multi-segmental model allowed us to define angular
281 displacement for each joint based on the data recorded by the motion capture system.

282 Force and moment data from the force plate were used to measure dynamic external force
283 exposures during each trial. Inertial moment contributions of the head and vertebral bodies were
284 added to the force plate measured moments and served to define the total external moment.

285

286 2.2.4.1 Muscle EMG Data Acquisition

287 EMG activities of the four pairs of extensor/flexor neck muscles were recorded using surface
288 electrodes. These muscles consisted of: left/right obliquus capitis, left/right splenius, left/right
289 longissimus, and left/right sternocleidomastoid (Fig.5). These muscles were chosen since they
290 are all major power producing neck muscles based on their cross-section area, and functionality.

291 The EMG electrodes were located on the shaved skin based upon a study of the anatomical
292 description of muscle locations (Alizadeh et al, 2016). The skin preparation was similar to
293 previously published paper (Marras and Davis, 2001).

294

295 An MRI imaging session was scheduled after the experimental session in order to
296 precisely document the anatomical features of the vertebral bodies. T1 and T2 weighted MRI
297 images were acquired on a 3T MRI scanner (Magnetom Trio, Siemens Healthcare, Erlangen,
298 Germany). Transverse slices of 1 mm thickness were obtained from the skull level and extended
299 caudally to the level of the second thoracic vertebra. This imaging session was also used to
300 validate the EMG electrode and optical marker location. The locations of the EMG electrodes
301 were indicated with diagnostic MRI markers. These markers showed up well in the imaging
302 allowing each electrode to be paired with the correct target muscle. In addition, custom made
303 dual modality markers were used to line up optical motion capture data with the MRI data. These
304 consisted of diagnostic MRI markers embedded within optical motion capture markers (Fig.6).

305 **3 Results**

306 3.1 Validation

307 Based on the findings of Dufour et al. (2013), the acceptable range for gain ratio of 6-131
308 N/cm^2V was adopted to represent the physiological acceptable range of gain in humans (Granata
309 and Marras, 1993). The gain ratio for each muscle calculated in this study was between 30-80,
310 which fell within the predicted physiological range previously reported for human spine.

311 The reliability of the model was investigated by comparing the resultant dynamic measured
312 external (to the body) moment to the predicted internal moment produced by the muscles and
313 ligaments in both the sagittal and axial planes via their correlation coefficient (R^2) and average

314 absolute error (AAE). Comparison of the measured external moment and the predicted internal
315 moment (over time) is illustrated in Figure 7. Since the moments generated in the lateral planes
316 were negligible compare to sagittal and axial planes, most probably signals are basically noise.
317 Therefore, planar R^2 would not be an appropriate measure for lateral plane. The model performed
318 well with a 0.73 weighted R^2 value in all three planes, considering each plane contribution in
319 generated moment. The weighted average absolute error of the predicted moment was less than
320 10% of the external moment in the calibration trial.

321 3.2 Spinal load

322 Figure 8 shows the peak spinal load at all the levels during the trial. The injury force tolerance
323 threshold for canine cervical spine has not been defined. Therefore, we will only comment on the
324 spine loading pattern in a relative fashion. Compression forces gradually increased from C1/C2
325 to C5/C6 where they were the greatest then these forces gradually decreased to C7/T1. The
326 anterior/posterior (A/P) and lateral (Lat) forces varied along the length of the cervical spine.

327 4. Discussion

328 It must be emphasized that all models, in general, are simplifications of a real situation.
329 However, for the first time, we have been able to develop a dog-specific cervical spine
330 biomechanical model that helps us understand the pattern of 3D moments and forces imposed
331 upon the vertebral tissues of the spine during a complex dynamic exertion made by a live animal.
332 The model developed by the authors was an EMG-driven hybrid model that predicted muscle
333 generated moments and determined spinal loads. EMG signals were used as a measure to
334 document the physiological pattern of muscle recruitment and optimization algorithms were
335 implemented in order to personalize the model by comparing moments about three axes of the

336 vertebral joints. The proposed model attempted to accurately and realistically represent the
337 mechanical loading and behavior of the neck structure, The EMG-driven canine neck model
338 predicted spinal loads as a result of twelve major canine neck muscle activities as a response to
339 physical exertions and external loads. The model was capable of estimating compression,
340 anterior/posterior, and lateral shear forces of the canine cervical spine at each level from C1-T1.
341 In order to interpret injury risk based on calculated spinal loads, canine specific disc failure
342 threshold values would be needed. Unfortunately, such information is not available in the
343 literature. One might consider adopting human threshold limits as a surrogate. However, the
344 extreme difference between human and canine cervical spine in many aspects such as the range
345 of motion, material properties, and disc size, would suggest that this may not be a reasonable
346 quantitative comparison.

347 The compression spine loads indicated a reasonable and expected pattern of loading,
348 where the highest compression values occurred at the C4/C5 level, similar to that reported by
349 Yoganandan et al., (2001) in the human cervical spine. It is not advisable to validate model
350 fidelity by quantifying spinal loads magnitude, since there is no experimental data on canine
351 cervical spine failure threshold to our knowledge. Moreover, due to the significant differences
352 between human and canine cervical spine ranging from tissue material properties to postural
353 variation and type of physical activities they are exposed to, it is not reasonable to compare them.
354 A similar argument can be made for the muscle forces and moments. One might consider the
355 magnitude of internal moments and spinal loads observed during the trial (Fig. 8) to be very
356 large. However, when considering the fact that the dog was pulling forcefully against a strong
357 latex resistance band, these spine loading magnitudes are not out of the range of possibilities in
358 the exertions may be close to a maximum exertion for the animal.

359 The current EMG-driven dynamic model is unique in that it was dog specific in terms of:
360 (1) muscle morphometric properties such as CSA, (2) muscle line of action, (3) muscle activities,
361 and (4) subject kinematics. The model structure is multi-dimensional and is capable of
362 considering dynamic responses of the subject. Neck moments and tissue loads are derived from
363 dynamic muscle force vectors and internal neck muscle moment arms. These parameters were
364 estimated based upon the EMG activity of 12 cervical spine muscles during the physical
365 exertion, while considering muscle moment generation potential which greatly depends on the
366 motion of the different canine body segments and resulting muscle moment arms. The surface
367 EMG signals of the major force producing muscles of the canine neck, along with muscle force-
368 length and force-velocity relationships were employed to estimate muscle forces.

369 This model represents a significant advancement in understanding the biomechanics of
370 canine cervical spine in several respects. First, this is a multi-segmental cervical spine model in
371 which Skull-T1 motion segments are separated and are allowed to move relative to each other.
372 The advantage of the multi-segmental cervical spine can be emphasized at the atlanto-occipital
373 and atlanto-axial joints. According to (Dugailly et al., 2011), 40% of axial rotation occurs at the
374 atlanto-axial joint, with the rest being distributed along the rest of the neck. This allowed us to
375 define angular displacement for each joint based on the data recorded by the motion capture
376 system. As a result, the error introduced into the model by implementing the calculated joint
377 angles from the recorded data of motion capture system was less than 0.5 mm. Therefore, the
378 model motion was almost identical to the actual dog motion. It is believed that while the joint
379 kinematics are precisely defined in the model, muscle moment arm and consequently measured
380 internal moment at each time point during the trial will be estimated more accurately.

381 Second, the exertion that was used for calibration and later was modeled represents a
382 complex motion including axial rotation and lateral bending while the dog was fully extending
383 his neck from a deep flexed posture, since constraining the dog to a specific range of motion was
384 impossible based upon the objective of the experiment which was to let the dog activate the neck
385 muscles naturally while performing extreme range of motion exertions. Therefore, it can be
386 claimed that the model is strong enough to respond a complex motion in spite of the model
387 limitations.

388 Third, a non-MVC calibration technique was used to determine personalized muscle gain
389 ratios. Since it would be impossible to obtain a true MVC in a canine specimen, and even in
390 humans MVCs can be sensitive to fatigue, posture, exertion type and pain on the exertion, the
391 non-MVC calibration technique proved to be very affective. The fidelity and robustness of this
392 technique is well established over a variety of complex exertions for humans (Dufour et al.,
393 2013). As described in the method section, in the presented model upper and lower bounds for
394 gain ratio was set based on the range reported by Dufour et al., (2013). We believe even though
395 this range was obtained for human lumbar spine, it is expected to be valid for this individual
396 canine since determined gain ratios were well within the boundaries. Further studies will need to
397 be performed to determine physiological gain ratio limits for canines.

398 Fourth, the muscle lines of action were determined in a cadaver-based experiment with a
399 precise technique. The advantages of this technique in comparison to the previously established
400 cadaver experiments were: 1) muscle measurements such as cross sectional area were achieved
401 without disturbing muscle attachments, 2) muscle cross sectional areas could be measured at any
402 level, and 3) estimated muscle lines of action were represented realistically since they were fitted

403 to the muscle centroid curve created by connecting muscle centroids in various planes, corrected
404 for muscle fibers angle.

405 As with any assessment tool one must appreciate the limitations of the model. First, it
406 should be noted that this model was developed based on data from a single animal subject.
407 Therefore, the estimated muscle properties including initial muscle length, CSA, line of action
408 are unique to this animal and are not necessarily representative of all canines. Another limitation
409 associated with the performance of the model is that at the beginning of the trial a strong
410 correlation between the predicted and measured moments were not observed. However, one must
411 consider that during the first quarter of the trial, the dog was not pulling against the latex band
412 due to the deep flexed posture of the neck. Thus, measured external moments for this portion of
413 the task were negligible, while internal moments were registered from the muscles. This
414 discrepancy may be due to limitations in the way inertial characteristics were estimated for the
415 head and vertebrae. Better approximations for these unknown variables will need to be
416 determined in the future. In addition, there were several parameters in the model such as gain
417 ratio constraints and ligament material properties that had been taken from a well-established
418 human spine model. Further investigation is necessary to determine more representative
419 parameters for canines. Finally, further exploration should be done in order to model atlanto-
420 occipital and atlanto-axial joints physiologically matched with proper tissue properties for canine
421 cervical spine. In spite of these procedural limitations, we believe this effort represents a
422 significant step forward in quantifying spine loads within the spine of a canine.

423

424 **5. Conclusions**

425 The model described in this article is the first known EMG-driven model for the canine cervical
426 spine. We believe the presented model is an important achievement in terms of application of
427 engineering principals to veterinary medicine. The developed model represents a significant step
428 toward implementing biomechanical modeling capabilities to understand underlying mechanisms
429 of the canine cervical spine non-invasively, although there are still many unknowns relative to
430 the canine cervical spine including kinematics and kinetics (Johnson et al., 2011). The model
431 met the objectives well by being able to track the motion precisely, accurately predict internal
432 moments of cervical spine based on the measured external moments, and estimate spinal tissue
433 loads that are reasonable based on the task that was performed. It is believed this model
434 represents a significant step toward building advanced canine biomechanical cervical spine
435 models for future investigations. Such an advanced canine specific model could be eventually
436 used by veterinary orthopedic and rehabilitation centers routinely to evaluate treatment strategies
437 and surgical techniques before applying them on the canine patient.

438 **Conflict of interest statement**

439 None declared.

440 **Acknowledgements**

441 This work was supported in part by Fitzpatrick Referrals Ltd., through the One Health/One
442 Medicine Fellowship at The Ohio State University.

443 **References**

444 Alizadeh, M., Zindl, C., Allen, M.J., Knapik, G.G., Fitzpatrick, N., Marras, W.S., 2016. MRI Cross Sectional
445 Atlas of Normal Canine Cervical Musculoskeletal Structure. Submitted for publication.

446 Autefage, A., Palierne, S., Charron, C., Swider, P., 2012. Effective mechanical properties of diaphyseal
447 cortical bone in the canine femur. *Vet. J. Lond. Engl.* 1997 194, 202–209.
448 doi:10.1016/j.tvjl.2012.04.001

449 Breit, S., Künzel, W., 2004. A Morphometric Investigation on Breed-Specific Features Affecting Sagittal
450 Rotational and Lateral Bending Mobility in the Canine Cervical Spine (C3–C7). *Anat. Histol.*
451 *Embryol.* 33, 244–250. doi:10.1111/j.1439-0264.2004.00546.x

452 Choi, H., Vanderby Jr, R., 1999. Comparison of Biomechanical Human Neck Models: Muscle Forces and
453 Spinal Loads at C4/5 Level. *J. Appl. Biomech.* 15, 120–138. doi:10.1016/S1350-4533(02)00151-0

454 Cholewicki, J., McGill, S.M., 1994. EMG assisted optimization: A hybrid approach for estimating muscle
455 forces in an indeterminate biomechanical model. *J. Biomech.* 27, 1287–1289. doi:10.1016/0021-
456 9290(94)90282-8

457 Cholewicki, J., McGill, S.M., Norman, R.W., 1995. Comparison of muscle forces and joint load from an
458 optimization and EMG assisted lumbar spine model: towards development of a hybrid approach.
459 *J. Biomech.* 28, 321–331.

460 Crisco, J.J., Panjabi, M.M., Wang, E., Price, M.A., Pelker, R.R., 1990. The injured canine cervical spine
461 after six months of healing. An in vitro three-dimensional study. *Spine* 15, 1047–1052.

462 Dufour, J.S., Marras, W.S., Knapik, G.G., 2013. An EMG-assisted model calibration technique that does
463 not require MVCs. *J. Electromyogr. Kinesiol. Off. J. Int. Soc. Electrophysiol. Kinesiol.* 23, 608–613.
464 doi:10.1016/j.jelekin.2013.01.013

465 Dugailly, P.-M., Sobczak, S., Moiseev, F., Sholukha, V., Salvia, P., Feipel, V., Rooze, M., Van Sint Jan, S.,
466 2011. Musculoskeletal modeling of the suboccipital spine: kinematics analysis, muscle lengths,
467 and muscle moment arms during axial rotation and flexion extension. *Spine* 36, E413–422.
468 doi:10.1097/BRS.0b013e3181dc844a

469 Dumas, G.A., Poulin, M.J., Roy, B., Gagnon, M., Jovanovic, M., 1991. Orientation and moment arms of
470 some trunk muscles. *Spine* 16, 293–303.

471 Foss, K., da Costa, R.C., Moore, S., 2013. Three-dimensional kinematic gait analysis of Doberman
472 Pinschers with and without cervical spondylomyelopathy. *J. Vet. Intern. Med. Am. Coll. Vet.*
473 *Intern. Med.* 27, 112–119. doi:10.1111/jvim.12012

474 Granata, K.P., Marras, W.S., 1995. An EMG-assisted model of trunk loading during free-dynamic lifting. *J.*
475 *Biomech.* 28, 1309–1317.

476 Granata, K.P., Marras, W.S., 1993. An EMG-assisted model of loads on the lumbar spine during
477 asymmetric trunk extensions. *J. Biomech.* 26, 1429–1438. doi:10.1016/0021-9290(93)90093-T

478 Han, I.S., Kim, Y.E., Jung, S., 2012. Finite element modeling of the human cervical spinal column: Role of
479 the uncovertebral joint. *J. Mech. Sci. Technol.* 26, 1857–1864. doi:10.1007/s12206-012-0427-2

480 Horst, M.J. van der, Thunnissen, J.G.M., Happee, R., Haaster, R.M.H.P. van, Wismans, J.S.H.M., 1997. The
481 Influence of Muscle Activity on Head-Neck Response During Impact (SAE Technical Paper No.
482 973346). SAE Technical Paper, Warrendale, PA.

483 Huber, Z.E., 2013. Creation and Validation of a Dynamic, EMG-Driven Cervical Spine Model. The Ohio
484 State University.

485 Hyeonki Choi, R.V.J., 2010. Comparison of Biomechanical Human Neck Models: Muscle Forces and Spinal
486 Loads at C4/5 Level [WWW Document]. *Hum. Kinet. J.* URL
487 [http://journals.humankinetics.com/jab-back-issues/jabvolume15issue2may/comparison-of-](http://journals.humankinetics.com/jab-back-issues/jabvolume15issue2may/comparison-of-biomechanical-human-neck-models-muscle-forces-and-spinal-loads-at-c45-level)
488 [biomechanical-human-neck-models-muscle-forces-and-spinal-loads-at-c45-level](http://journals.humankinetics.com/jab-back-issues/jabvolume15issue2may/comparison-of-biomechanical-human-neck-models-muscle-forces-and-spinal-loads-at-c45-level) (accessed
489 12.17.15).

490 Jaeger, R., Mauch, F., Markert, B., 2011. The muscle line of action in current models of the human
491 cervical spine: a comparison with in vivo MRI data. *Comput. Methods Biomech. Biomed. Engin.*
492 15, 953–961. doi:10.1080/10255842.2011.567982

493 Jager, M. de, Sauren, A., Thunnissen, J., Wismans, J., 1996. A Global and a Detailed Mathematical Model
494 for Head-Neck Dynamics. Proceeding Thw 30th Stapp Car Crash Conf. SAE Paper No. 962430,
495 269–281.

496 Jaumard, N.V., Welch, W.C., Winkelstein, B.A., 2011. Spinal facet joint biomechanics and
497 mechanotransduction in normal, injury and degenerative conditions. *J. Biomech. Eng.* 133,
498 071010. doi:10.1115/1.4004493

499 Jeffery, N. d., Levine, J. m., Olby, N. j., Stein, V. m., 2013. Intervertebral Disk Degeneration in Dogs:
500 Consequences, Diagnosis, Treatment, and Future Directions. *J. Vet. Intern. Med.* 27, 1318–1333.
501 doi:10.1111/jvim.12183

502 Johnson, J.A., da Costa, R.C., Bhattacharya, S., Goel, V., Allen, M.J., 2011. Kinematic motion patterns of
503 the cranial and caudal canine cervical spine. *Vet. Surg. VS* 40, 720–727. doi:10.1111/j.1532-
504 950X.2011.00853.x

505 Jorgensen, M.J., Marras, W.S., Gupta, P., 2003. Cross-sectional area of the lumbar back muscles as a
506 function of torso flexion. *Clin. Biomech. Bristol Avon* 18, 280–286.

507 Kumar, M.S.A., 2012. Clinically Oriented Anatomy of the Dog and Cat. Linus Publications, Ronkonkoma,
508 NY 11779.

509 Lim, T.H., Goel, V.K., Weinstein, J.N., Kong, W., 1994. Stress analysis of a canine spinal motion segment
510 using the finite element technique. *J. Biomech.* 27, 1259–1269.

511 Lopik, D.W. van, Acar, M., 2007. Development of a multi-body computational model of human head and
512 neck. *Proc. Inst. Mech. Eng. Part K J. Multi-Body Dyn.* 221. doi:10.1243/14644193JMBD84

513 Macintosh, J.E., Bogduk, N., 1991. The attachments of the lumbar erector spinae. *Spine* 16, 783–792.

514 Marras, W.S., Davis, K.G., 2001. A non-MVC EMG normalization technique for the trunk musculature:
515 Part 1. Method development. *J. Electromyogr. Kinesiol. Off. J. Int. Soc. Electrophysiol. Kinesiol.*
516 11, 1–9.

517 Marras, W.S., Granata, K.P., 1997. The development of an EMG-assisted model to assess spine loading
518 during whole-body free-dynamic lifting. *J. Electromyogr. Kinesiol. Off. J. Int. Soc. Electrophysiol.*
519 *Kinesiol.* 7, 259–268.

520 McCully, K.K., Faulkner, J.A., 1983. Length-tension relationship of mammalian diaphragm muscles. *J.*
521 *Appl. Physiol.* 54, 1681–1686.

522 Németh, G., Ohlsén, H., 1986. Moment arm lengths of trunk muscles to the lumbosacral joint obtained
523 in vivo with computed tomography. *Spine* 11, 158–160.

524 Sharir, A., Milgram, J., Shahar, R., 2006. Structural and functional anatomy of the neck musculature of
525 the dog (*Canis familiaris*). *J. Anat.* 208, 331–351. doi:10.1111/j.1469-7580.2006.00533.x

526 Sheng, S.-R., Wang, X.-Y., Xu, H.-Z., Zhu, G.-Q., Zhou, Y.-F., 2010. Anatomy of large animal spines and its
527 comparison to the human spine: a systematic review. *Eur. Spine J. Off. Publ. Eur. Spine Soc. Eur.*
528 *Spinal Deform. Soc. Eur. Sect. Cerv. Spine Res. Soc.* 19, 46–56. doi:10.1007/s00586-009-1192-5

529 Snijders, C.J., Hoek van Dijke, G.A., Roosch, E.R., 1991. A biomechanical model for the analysis of the
530 cervical spine in static postures. *J. Biomech.* 24, 783–792.

531 Soret, M., Bacharach, S.L., Buvat, I., 2007. Partial-volume effect in PET tumor imaging. *J. Nucl. Med. Off.*
532 *Publ. Soc. Nucl. Med.* 48, 932–945. doi:10.2967/jnumed.106.035774

533 Stemper, B.D., Yoganandan, N., Pintar, F.A., 2004. Validation of a head-neck computer model for
534 whiplash simulation. *Med. Biol. Eng. Comput.* 42, 333–338.

535 Theado, E.W., Knapik, G.G., Marras, W.S., 2007. Modification of an EMG-assisted biomechanical model
536 for pushing and pulling. *Int. J. Ind. Ergon., Musculoskeletal Load of Push–Pull Tasks* 37, 825–831.
537 doi:10.1016/j.ergon.2007.07.012

538 Vasavada, A.N., Li, S., Delp, S.L., 1998. Influence of muscle morphometry and moment arms on the
539 moment-generating capacity of human neck muscles. *Spine* 23, 412–422.

540 Zimmerman, M.C., Vuono-Hawkins, M., Parsons, J.R., Carter, F.M., Gutteling, E., Lee, C.K., Langrana,
541 N.A., 1992. The mechanical properties of the canine lumbar disc and motion segment. Spine 17,
542 213–220.

543

544

545

546

547

548

549

550

551

552

553

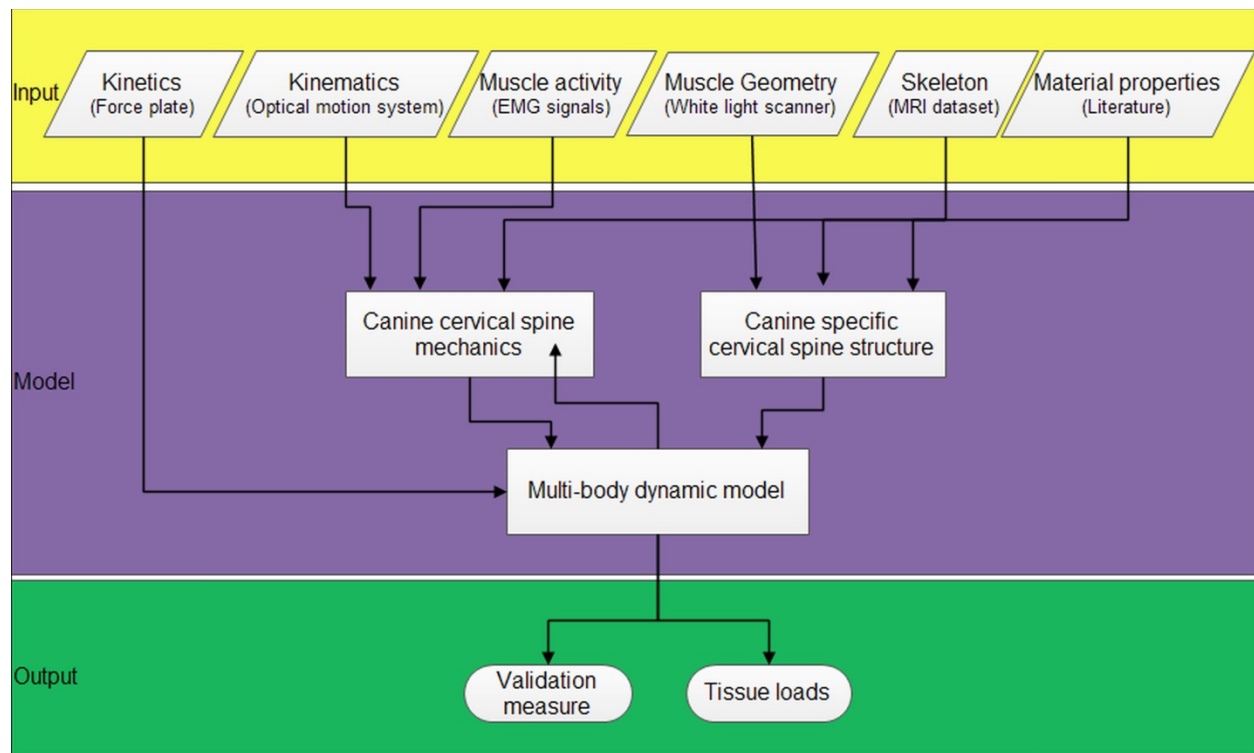
554

555

556

557

558



559

560 **Figure.1** This graphic displays the overall modeling logic.

561

562

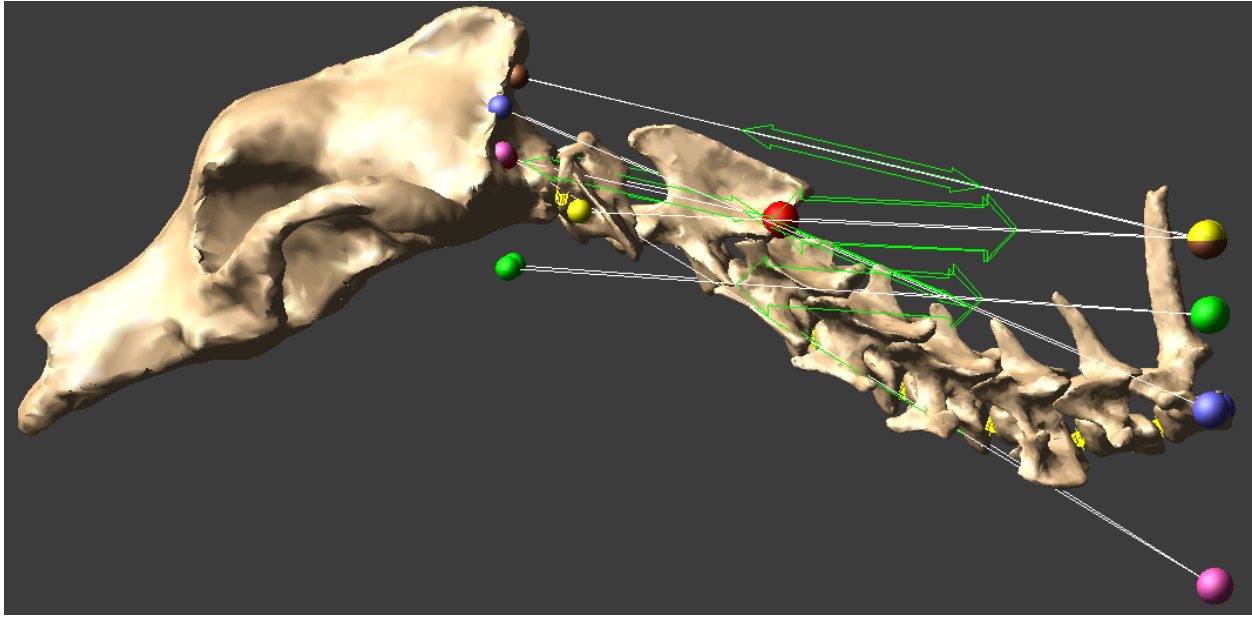
563

564

565

566

567



568

569 **Figure 2.** Dynamic model of canine cervical spine with straight line muscles. (a) Side view. (b)

570 Top view. ● longissimus, ● complexus, ● sternocleidomastoid, ● splenius, ● obliquus capitis,

571 ● biventer.

572



573

574 **Figure 3.** The latex resistance band (TheraBand, Akron, OH, USA) connected to the neck of the
575 subject from one end and to the force plate from the other end. The subject was naturally pulling
576 against the latex resistance band in order to eat the food treat.

577

578

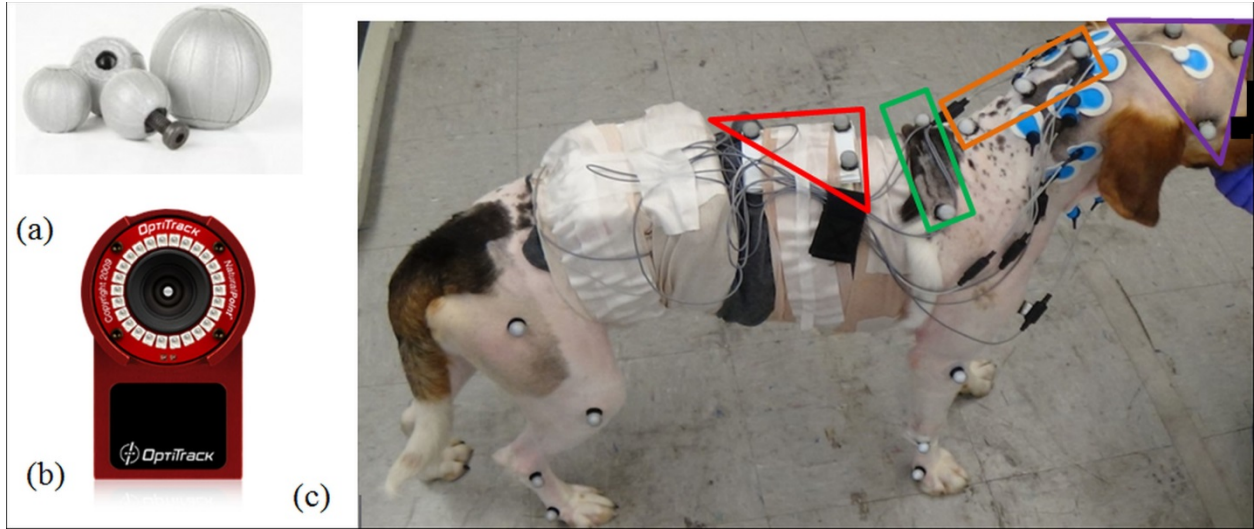
579

580

581

582

583



584

585 **Figure 4.** (a) Optical markers. (b) Optical motion capture camera. (c) Location of optical
586 markers in order to measure joint angles: \blacktriangle Head markers, \square Neck markers, \square Shoulder markers, \blacktriangle
587 UpperTorso markers

588

589

590

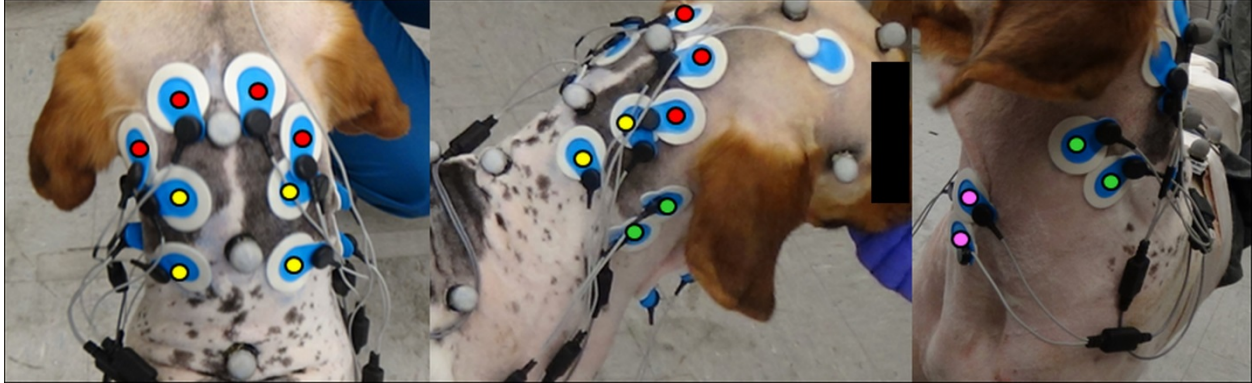
591

592

593

594

595



596

597 **Figure 5.** Surface electromyography (EMG) electrode location, ●Obliquus capitis, ●Splenius,

598 ● Longissimus, ● Sternocleidomastoideus

599

600

601

602

603

604

605

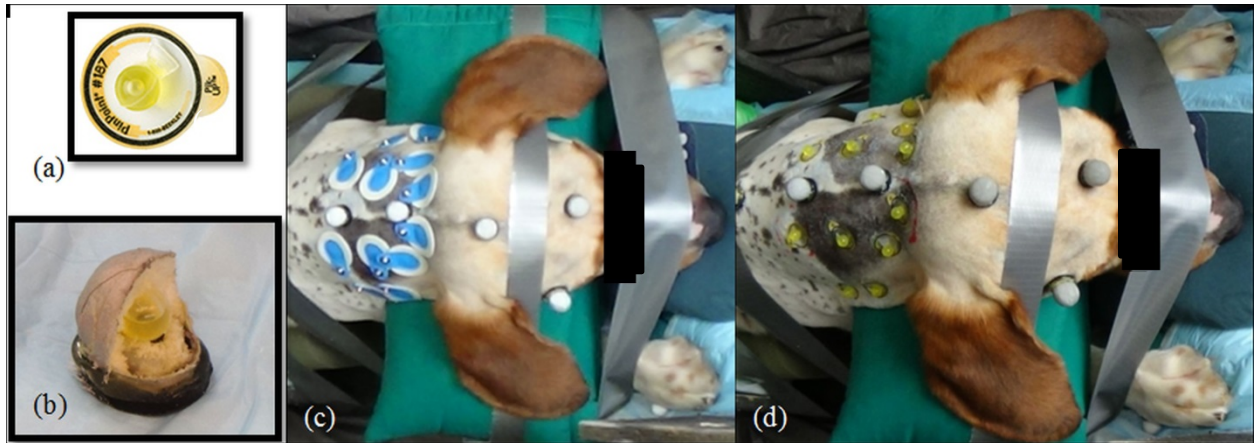
606

607

608

609

610



611

612 **Figure 6.** (a) MRI diagnostic marker, (b) Dual modality marker (cut in half for clarity), (c)
613 location of EMG electrodes and dual modality markers, (d) replaced EMG electrodes with MRI
614 diagnostic marker.

615

616

617

618

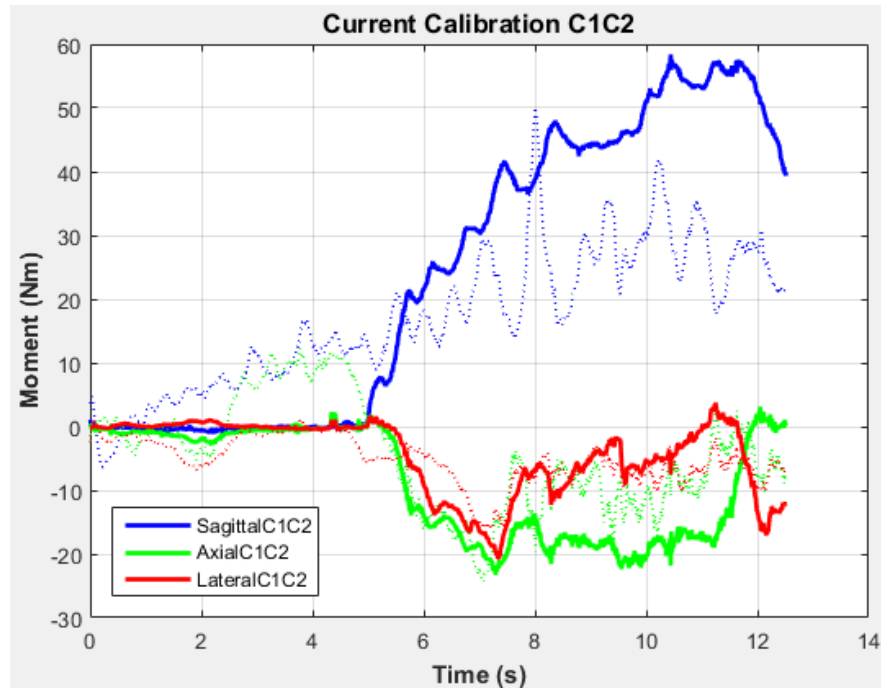
619

620

621

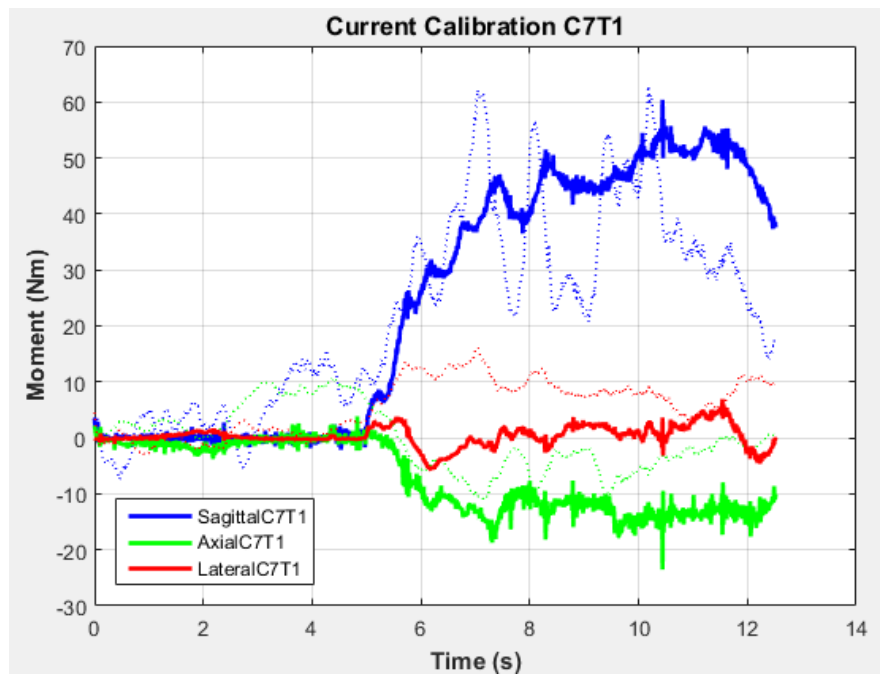
622

623



(a)

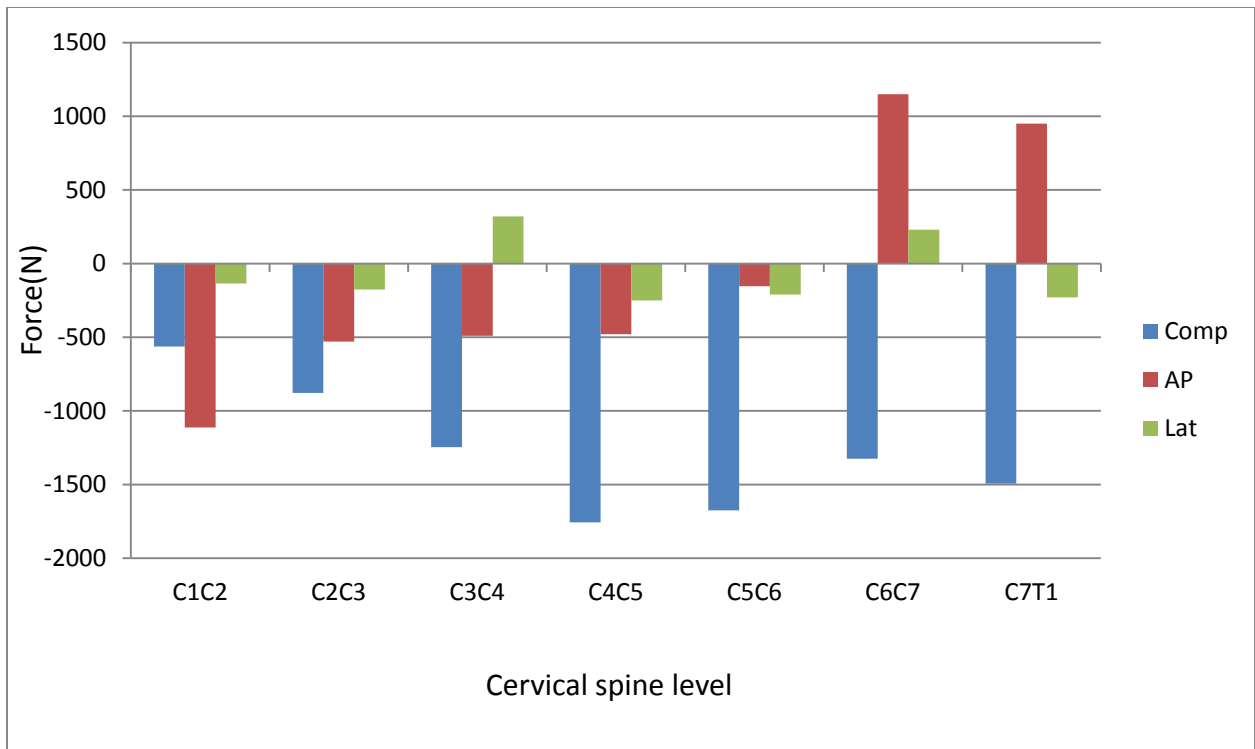
624



(b)

625

626 **Figure 7.** Canine cervical spine measured external moments (solid lines) as a function of time
 627 during a typical exertion and the moments predicted from the EMG-assisted model for the
 628 calibration trial (dashed lines). (a) C1C2 level. (b) C7T1 level. Blue = Sagittal plane, Green =
 629 Axial plane, Red = Lateral plane.



630

631 **Figure 8.** Maximum Spinal load during the trial at each level (comp=Compression,
 632 AP=Anterior-posterior shear, Lat= Lateral shear).

633